ATTITUDE CONTROL PERFORMANCE OF IRVE-3

Robert A. Dillman,[*] Valerie T. Gsell, Ernest L. Bowden[†]

The Inflatable Reentry Vehicle Experiment 3 (IRVE-3) launched July 23, 2012, from NASA Wallops Flight Facility and successfully performed its mission, demonstrating both the survivability of a hypersonic inflatable aerodynamic decelerator in the reentry heating environment and the effect of an offset center of gravity on the aeroshell's flight L/D. The reentry vehicle separated from the launch vehicle, released and inflated its aeroshell, reoriented for atmospheric entry, and mechanically shifted its center of gravity before reaching atmospheric interface. Performance data from the entire mission was telemetered to the ground for analysis. This paper discusses the IRVE-3 mission scenario, reentry vehicle design, and as-flown performance of the attitude control system in the different phases of the mission.

INTRODUCTION

The Inflatable Reentry Vehicle Experiment 3 (IRVE-3) launched July 23, 2012, from NASA Wallops Flight Facility (WFF) on a Black Brant XI suborbital sounding rocket and successfully performed its mission, demonstrating both the survivability of a hypersonic inflatable aerodynamic decelerator (HIAD) in the reentry heating environment and the effect of an offset center of gravity on the HIAD's lift-to-drag ratio. IRVE-3 was a follow-on mission to IRVE-II, which in August 2009 made the first fully successful flight of a HIAD, demonstrating exo-atmospheric inflation, reentry survivability – without significant heating – and the aerodynamic stability of a HIAD down to subsonic flight conditions. NASA Langley Research Center is leading the development of HIAD technology for use on future interplanetary and Earth reentry missions.

MISSION DESCRIPTION

As shown in Figure 1, the IRVE-3 mission performed a yo-yo de-spin after burnout of the upper stage of the launch vehicle, then separated from the rocket motor and released the nose cone. The vehicle then coasted through space for over five minutes, passing through apogee at 469km, before the on-board timer triggered the release of the aeroshell's launch restraint cover and signaled the inflation system to begin pressurizing the aeroshell. The inflation system used high-pressure nitrogen to fill the aeroshell to 138 KPa (20psi), deploying the inflatable to its full 3m diameter, and maintained inflation at that level above ambient conditions through reentry and the end of the flight experiment. Immediately prior to atmospheric interface, the attitude control sys-

---

tem reoriented the vehicle to the desired nose-first reentry attitude, and the center-of-gravity (CG) offset mechanism shifted the aft portion of the metal centerbody to one side, shifting the vehicle CG to induce an angle of attack and a lateral lift vector during reentry.
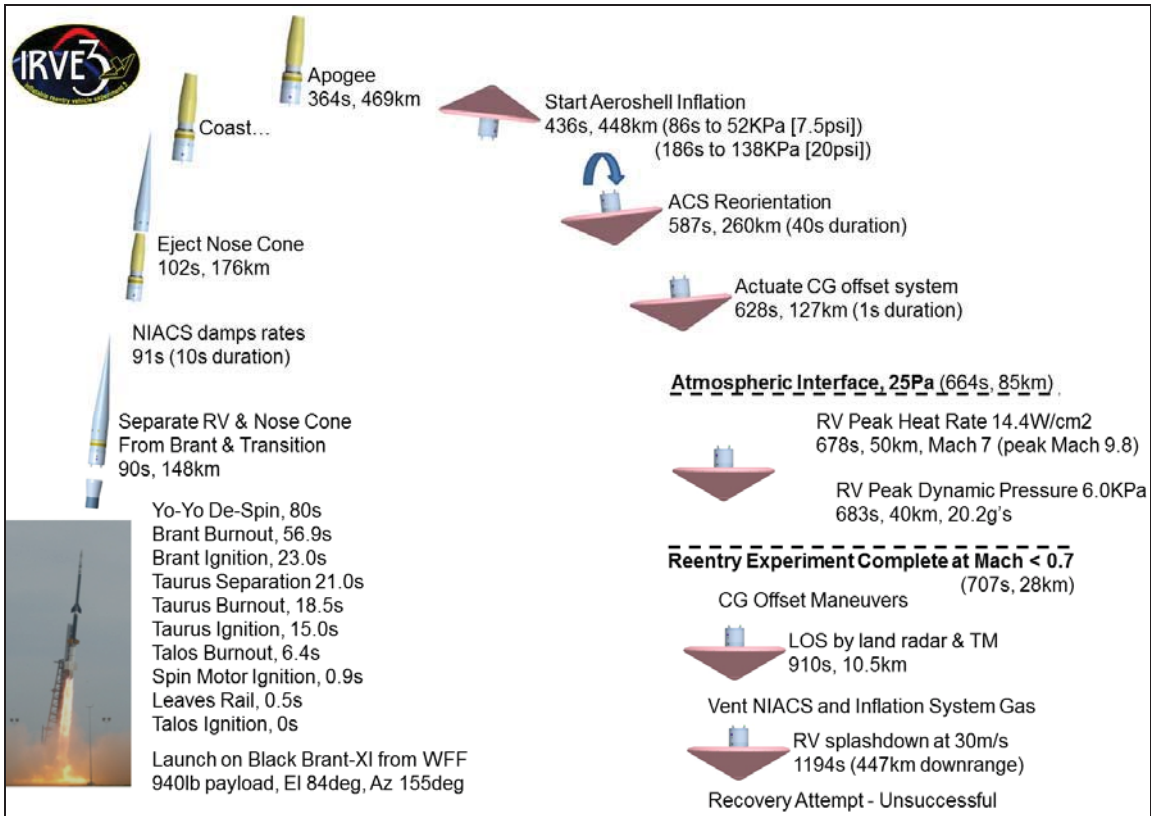

Figure 1: IRVE-3 Flight Event Summary.

The IRVE-3 vehicle reentered Earth's atmosphere at over 2700m/s, approximately Mach 10. During reentry, the vehicle endured a peak deceleration of 20G's and a maximum heat flux of slightly over 14W/cm2. While the heating did not reach the levels seen in orbital and interplanetary entry missions, it provided a relevant test for the flexible TPS covering the inflatable aeroshell, which uses a high drag area and resulting low ballistic coefficient to reduce the peak flux seen during reentry. IRVE-3 accomplished all of its mission objectives during the flight. After slowing below Mach 0.7, the official end of the flight experiment, the CG offset mechanism performed a series of CG shifts to allow additional measurements of the aerodynamic response time of the inflatable aeroshell to CG control maneuvers. The reentry vehicle dropped below the horizon from the ground tracking stations at 10.5km altitude, 910 seconds after launch. Recovery of the vehicle was attempted with a spotter plane guiding a recovery ship, but was unsuccessful.

During the IRVE-3 mission the attitude control system (ACS) performed several different functions critical to the mission. The ACS damped out the remaining spin and tumble after yo-yo de-spin and separation of the reentry vehicle from the upper stage motor, so that the nose cone could be ejected without unnecessary rotational dynamics. Prior to reentry, the ACS reoriented the IRVE-3 reentry vehicle from the nose-up launch orientation to the nose-down entry orientation, at the predicted nominal angle of attack for the aeroshell. During reentry, the ACS turned off pitch and yaw control to allow measurement of the aerodynamic stability of the vehicle, but maintained roll control so the lift vector would point in the desired direction. Finally, the ACS

2

and the inflation system both vented their pressurized tanks shortly before splashdown, to safely allow the recovery team to approach the vehicle after splashdown.

REENTRY VEHICLE DESCRIPTION

As shown on the left side of Figure 2, the reentry vehicle launched with the inflatable aeroshell folded forward and packed in a roughly conical shape to fit inside the launch vehicle nose cone. The rigid nose of the reentry vehicle was underneath the stowed aeroshell, and was followed in order by the inflation system, the CG offset mechanism, the telemetry module, the attitude control system, and the cameras used to observe the in-flight behavior of the inflatable aeroshell.
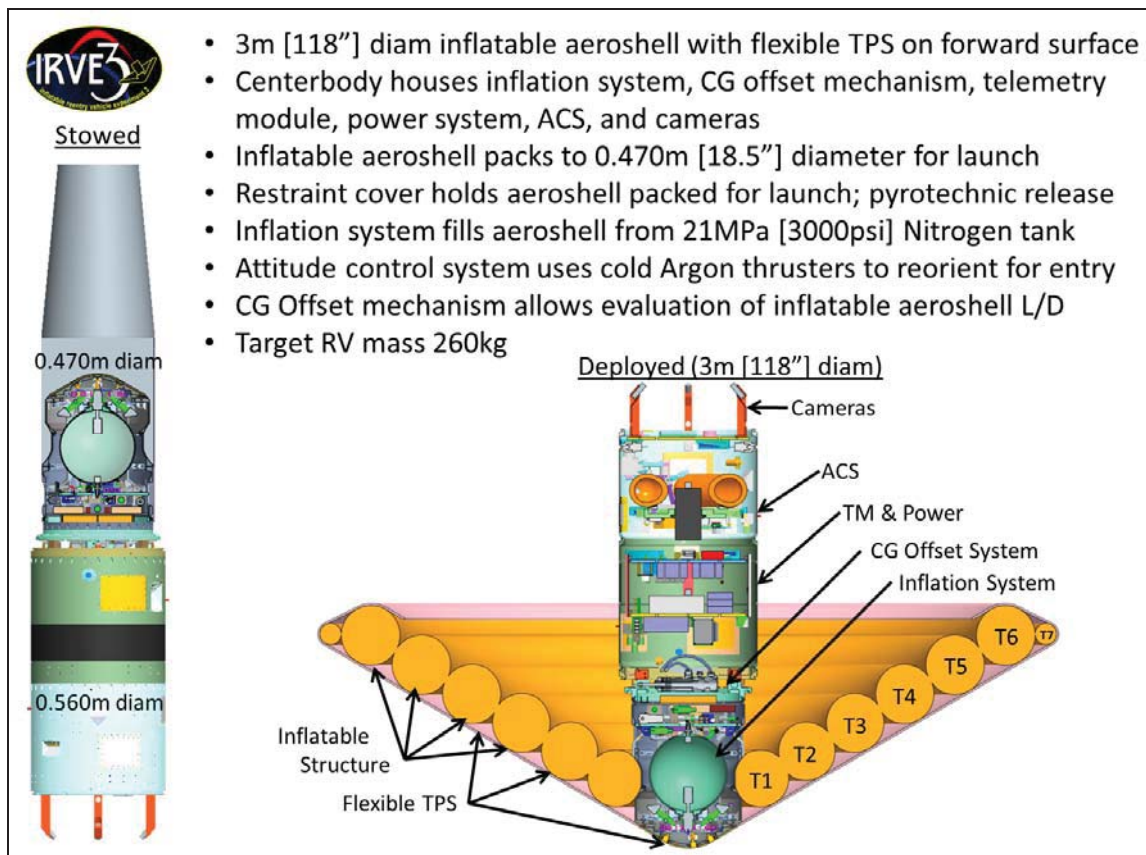

Figure 2: Reentry Vehicle Configurations.

The inflatable aeroshell used seven pressurized toroids covered with a high-temperature fabric thermal protection system (TPS) to produce a 3m [118"] diameter, 60 degree half angle reentry cone. The same fabric TPS also covered the rigid nose of the vehicle, where the flight environment was monitored using five heat flux gauges with integrated pressure sensors. Flight performance of the TPS was measured by 18 thermocouples embedded in the nose TPS, and 34 more on the aeroshell body. Additional instrumentation in the centerbody monitored the performance of the on-board systems and the trajectory of the vehicle. The flight data, including the video from the four video cameras, was telemetered to the ground for analysis and comparison with the radar data from ground tracking stations.

CONTROL SYSTEM DESCRIPTION

The ACS used for the IRVE-3 mission was the NIACS (NASA Sounding Rocket Operations Contract Inertial ACS). The NIACS consists of a pneumatic system that can be configured to support the gas needs of the mission, a 3-axis roll stabilized fiber optic gyroscope and a flight computer. IRVE-3 used two 3.3 liter (200 in[3]) composite overwrap gas tanks pressurized to 34 Mega Pascal (5000 psi) with Argon gas. The Argon was plumbed out to two pitch nozzles, two yaw nozzles and a roll manifold feeding two clockwise and two counterclockwise nozzles. A transfer solenoid selects a coarse or fine regulator based on control system logic. High or low pressure regulated gas was then fed to the nozzles. This allows for bi-level pneumatics control switched through software commanding of the transfer valve.
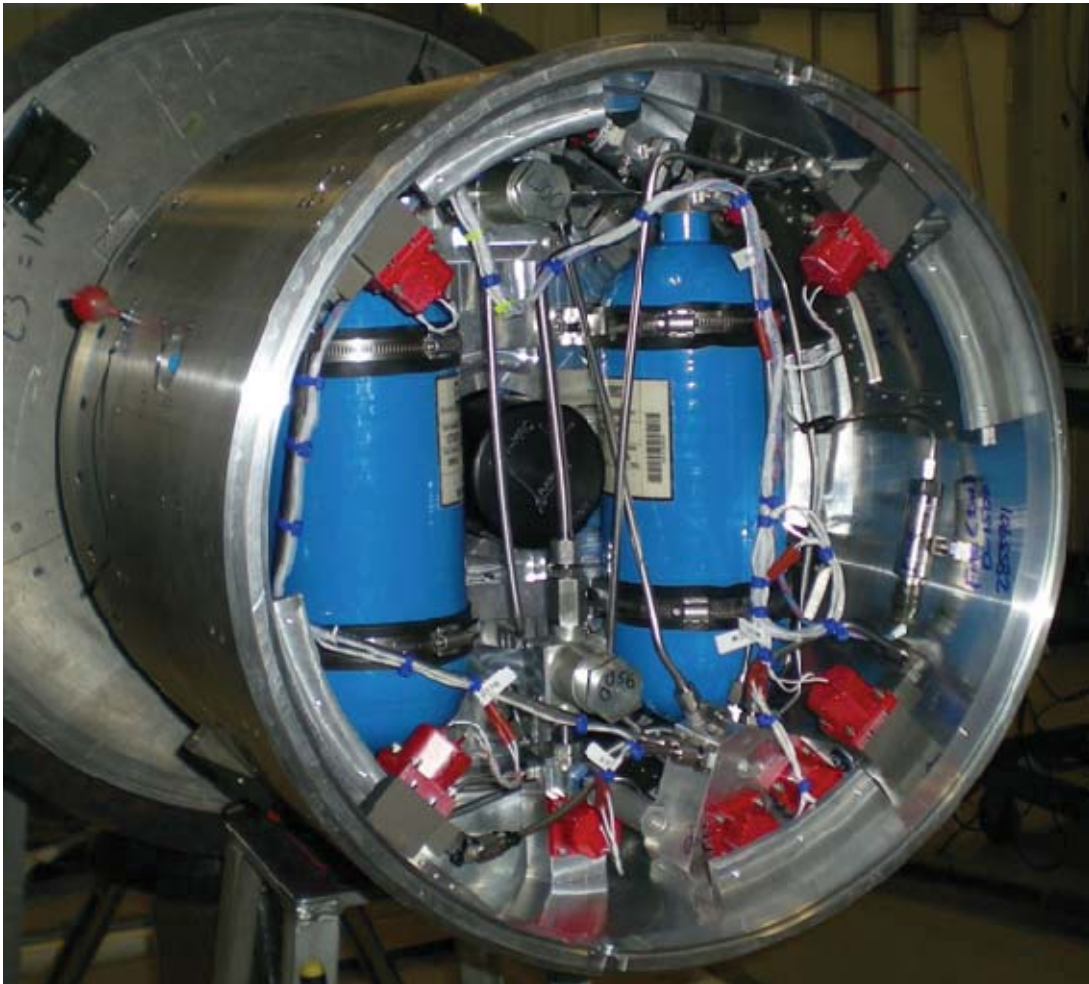

Figure 3: IRVE-3 ACS.

For this mission the NIACS received Earth fixed measures of the payload velocity and position from the onboard GPS. From that information the targeting was calculated. The IRVE-3 payload desired to have the aeroshell nose down and aligned along the payload velocity vector with rates about all three axes stabilized near zero. The roll orientation of the payload was aligned with the projection of forward velocity on the ground as illustrated in Figure 4. This zero

bank angle attitude allowed for the designed center of gravity to generate a lift vector with the maximum vertical component. Prior to entry, the NIACS was used to orient the inflated aeroshell along the velocity vector while damping all rates. The pitch and yaw control was then disabled for entry and the roll orientation was held through the peak deceleration and heating.
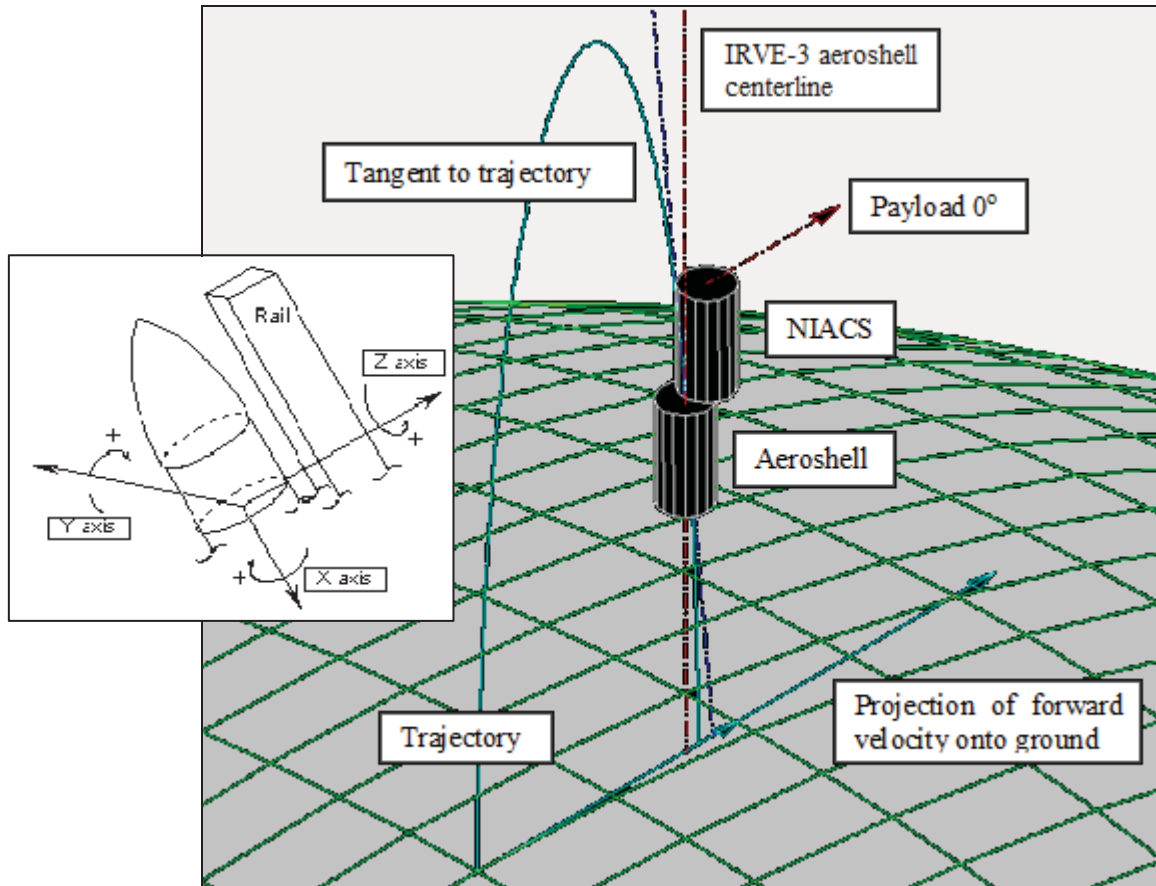

Figure 4: IRVE-3 Targeting and Coordinate System.

PREFLIGHT TESTING

The IRVE-3 ACS participated in three significant hardware testing efforts. First, the system was completely assembled and integrated into the full payload and the flight sequence of events was executed in an evacuated facility and the aeroshell was allowed to inflate. Second, the full payload was tested mechanically and electrically in the standard manner for all NASA sounding rocket payloads; the on-board systems are run through a sequence of all timed events before and after 3-axis vibration testing that simulates the environment of motor burn. Finally, the ACS was tested at the Wallops air bearing facility and the system demonstrated all flight maneuvers at the desired as well as high and low accelerations.

Complete System Test

In order to fully demonstrate the function of the all ground testable aspects of the IRVE-3 experiment, the full payload was brought to the Transonic Dynamics Tunnel facility at Langley Research Center. The TDT is a wind tunnel that is designed to be pumped down to a coarse vacuum of a few Kilopascals and then re-pressurized with heavy gasses for wind tunnel testing. IRVE-3 used this tunnel as a large vacuum chamber. The payload was placed in the tunnel, hard-

mounted to the floor, with the aeroshell fully packed and restrained. The tunnel was depressurized and the system timers were started, allowing mission events to be triggered autonomously as in flight. The ACS jets fired at their commanded times, simulating damping of the remaining motion after the yo-yo de-spin, orientation of the vehicle for reentry, and roll control during reentry. The pyrotechnic system simulated the release of the nose cone at the desired time. The aeroshell restraint cover was released, and the inflation system performed as desired, reaching full inflation pressure within the expected time. The CG offset system also performed as desired, shifting the aft portion of the centerbody back and forth on command.

This vacuum test was also used to fire a gas sequence from the ACS nozzles to observe the reaction of the aeroshell to the ACS jets. It was suspected that a small percentage of gas from the roll, pitch, and yaw nozzles would impact the aeroshell, and the effects of this were estimated and accounted for in the preflight simulation work. However, no effect of the ACS firings was observed during vacuum testing; there was no movement visible.

Environmental Testing

IRVE-3 was launched on a Black Brant XI 3 stage solid rocket vehicle. The payload was subject to the standard battery of tests for this class of sounding rocket launch vehicles. All payload sections were electrically and mechanically integrated and the launch event timer was initiated by the mechanical tripping of skin-mounted micro switches. The timely initiation and completion of all events was monitored along with housekeeping channels throughout the full test. The payload then underwent vibration testing. All three axes were subject to random vibration across a range of frequencies and the thrust axis was also tested in sine vibration. After the successful completion of vibration testing, all the flight event times and housekeeping were rechecked to ensure nominal operation. All deployments were also tested as well as proper operation while spinning the payload at the rotational rates expected during launch. The IRVE-3 payload successfully passed all tests and there were no ACS issues.

Air Bearing Testing

The ACS is tested at the Wallops horizontal air bearing facility. This allows for 100% of the flight hardware and software to be tested together executing the desired control. The air bearing has a full telemetry system and an onboard GPS simulator. Simulated GPS trajectories are fed to the air bearing receiver so that nominal and off nominal trajectories may be received by the ACS to well test GPS targeting. It is typically not possible to match the payload gravimetrics in all control configurations with the air bearing set up. Especially for 3-axis stabilized control it is more important to match the resultant accelerations than the specific gravimetrics from which those accelerations are derived. For IRVE-3, all control configuration accelerations were well matched on the air bearing, and the testing on air bearing was well matched to the preflight simulation work. In order to best predict the behavior of the control system during entry, the control logic was implemented into the IRVE-3 trajectory simulation at Langley. Air bearing sensor measurements were fed into this simulation and the simulation results were compared to the air bearing results. A step by step match was achieved giving high confidence that the controller had been properly implemented in the Langley simulation. Air bearing results were also compared to the standard NSROC simulation by matching the trajectory inputs and the initial attitude and rate conditions. This comparison was also favorable giving confidence that the control system was well characterized in the simulation. Examples of post flight simulation comparisons will be shown in the section following flight results.
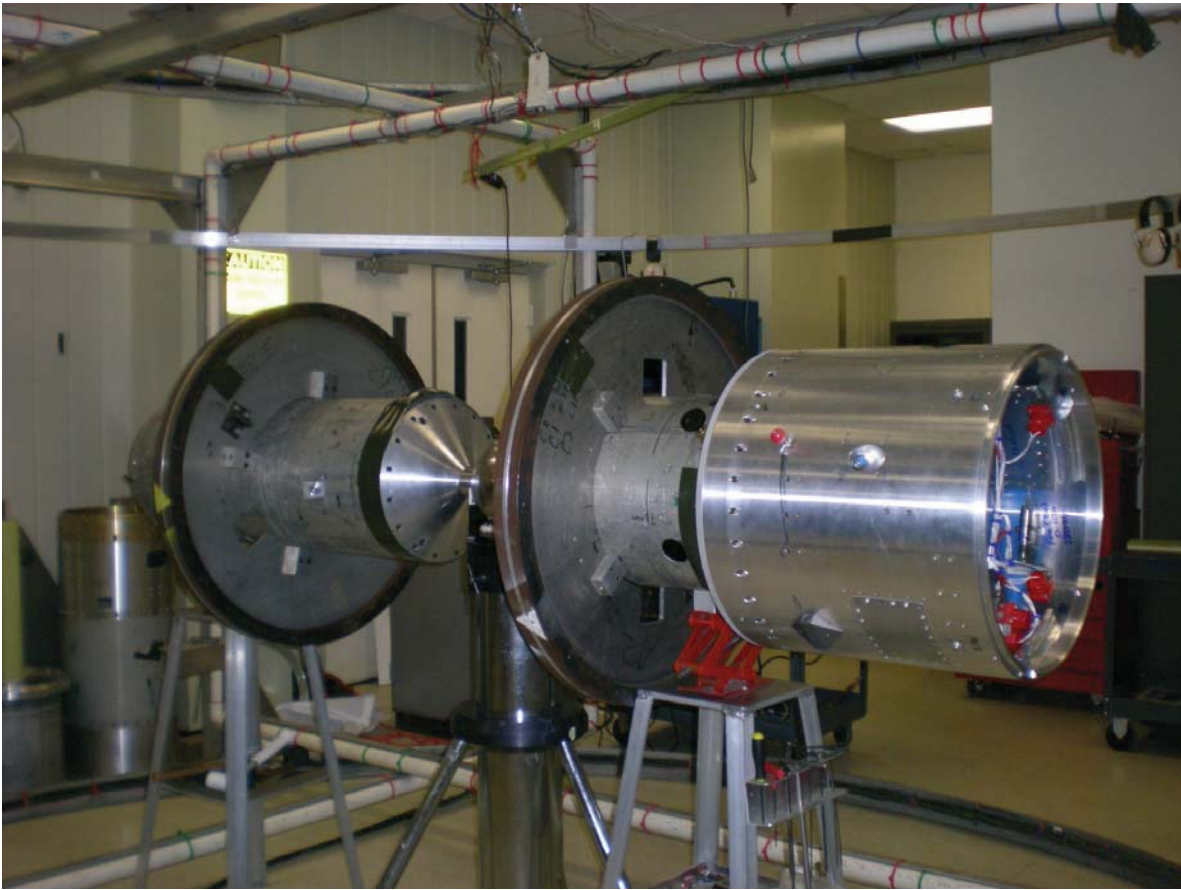
Figure 5: IRVE-3 on the Air Bearing.

FLIGHT RESULTS

Rate Damping for Nose Cone Deploy

In the event of anomalous motor burn or significant tip off from despin or motor separation, the ACS was enabled to damp the lateral and roll rates before nose cone deploy. The behavior of the 4 foot tall packed aeroshell stowed under the nosecone was not well characterized. While the NIACS is capable of rate damping in all axes to well below 1 degree/second, due to the unknown flexible response of the packed aeroshell, the rate damping limits were set at 1 degree per second in pitch and yaw and 5 degrees per second in roll. The intent was to allow for a sufficiently stable environment for nose cone separation without risking the ACS pneumatic activity exciting a flexible response from the aeroshell. This was successful. The rates at 91 seconds when the ACS is enabled for control were 22 degrees per second in roll and 1.2 degrees per second in pitch. The system stayed in coarse mode for 0.2 seconds and the rate damping was complete after 1.5 seconds. The nosecone separation was clean and no evidence of flexibility was seen in response to pneumatic activity. Motor separation is seen just after 90 seconds and nosecone deploy is seen just after 102 seconds.
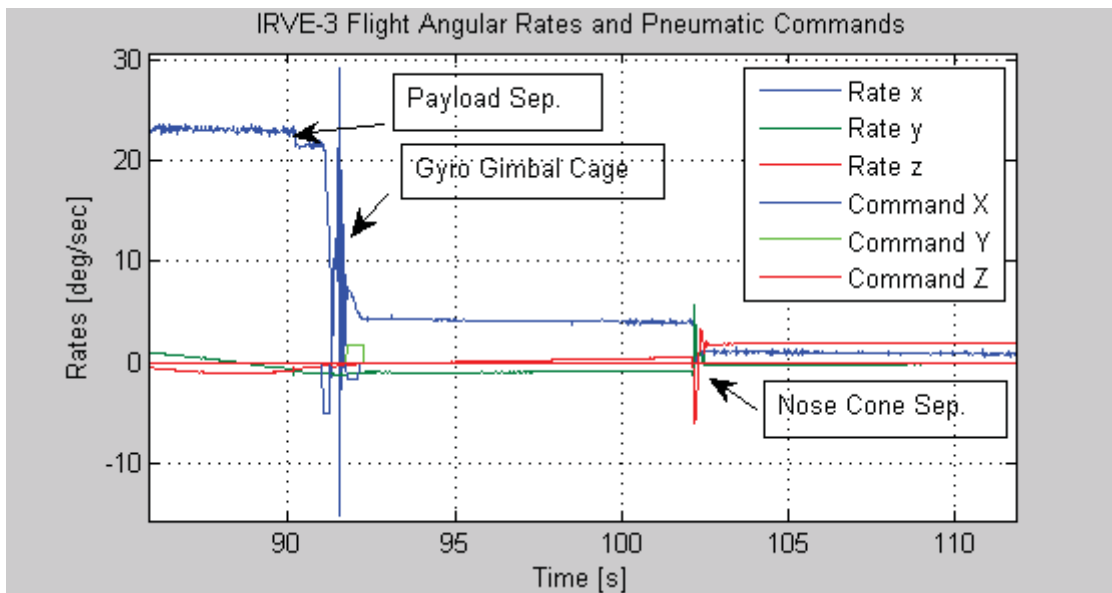
Figure 6: Rate damping for nose cone deploy.

Exoatmospheric Alignment

At T+429 seconds the retaining bag cutters are fired and the aeroshell is allowed to unfold. At T+436 seconds the inflation system comes on to begin the 200+ second process of inflating the aeroshell. The ACS is enabled at T+587 seconds to align the nose of the aeroshell to the desired measured target.
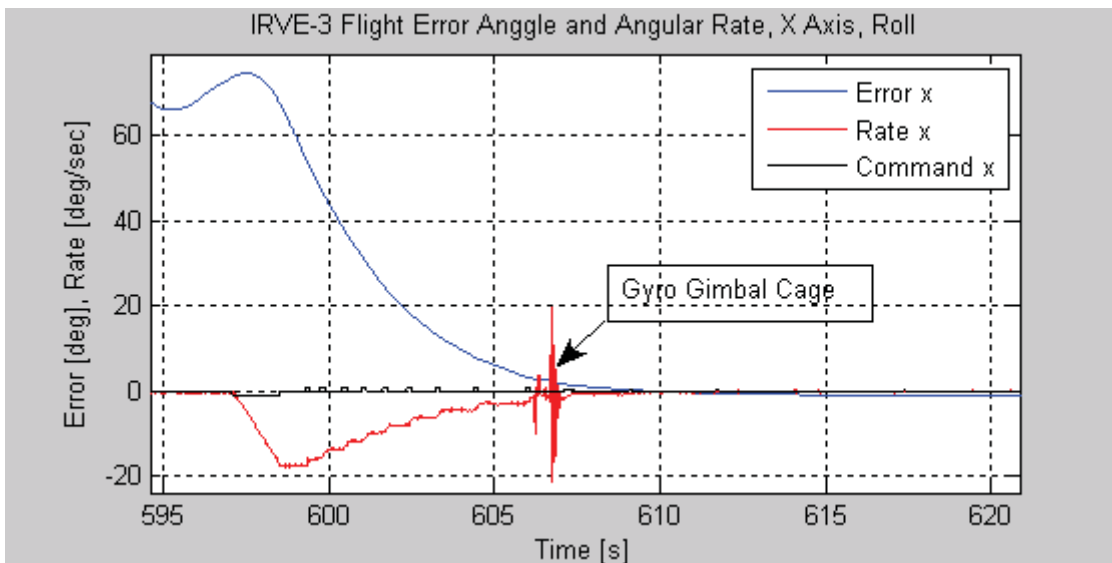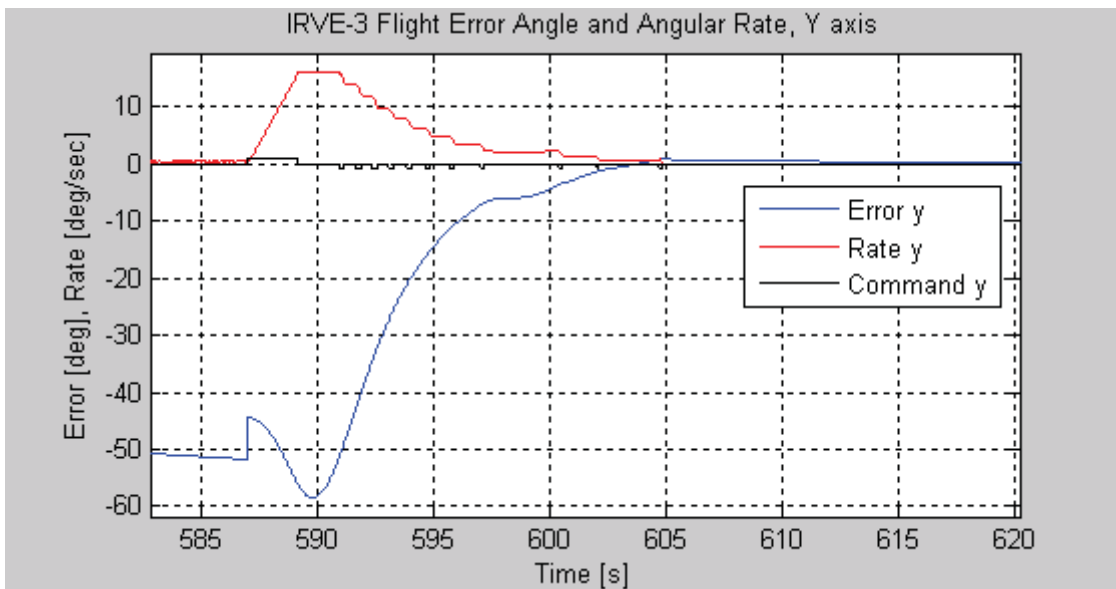

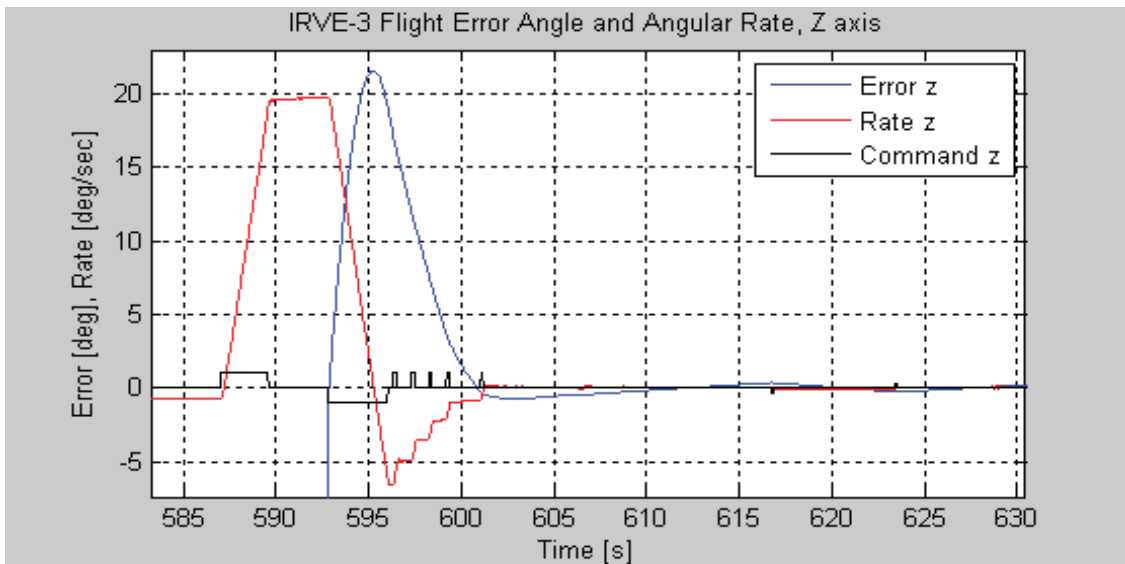**Figure 7: Initial convergence, roll.**

8

Figure 8: Initial convergence, Y.

Figure 9: Initial convergence, Z.

It was expected that the inflation process would take up to 220 seconds from preflight tests. This would put the aeroshell at about 50% inflated and at a stiffness of 75% of full inflation stiffness when the ACS begins control. The first rocking mode of the aeroshell attachment joint was predicted and then measured to be approximately 9 Hz at full inflation and 7 Hz at 50% inflation. Software filters were put in place on the control rates to filter out the resonant response of the aeroshell felt on the centerbody. This prevented the ACS from reacting to and ultimately driving the aeroshell at its resonant frequency. The first torsional mode of the aeroshell was predicted to be approximately 25 Hz, sufficiently high that there was less concern over ACS excitation in roll control due to the low expected frequency of roll nozzle firings. The torsional response was at a much higher gain than the rocking modes so good filtering was critical in the roll axis as well.

Both 3 and 5 Hz cutoff frequency filters were developed and tested in simulation and on the air bearing for the lateral rate channels. Both suggested good control performance and sufficient filtering in both the partial and fully inflated states. It was also observed that the 5 Hz filters would not sufficiently remove the flexible response in the under-inflated state. As a precaution, the 3 Hz filters were left in place on the pitch and yaw rates for the full control period should the aeroshell fail to achieve or maintain full inflation pressure. Due to the higher frequency of the torsional mode, 5 Hz filters were used for the roll channel. Figure 10 shows the rate filters working well at C/G offset. The aft portion of the centerbody was translated laterally along the NIACS Z axis, payload 0-180deg. This action resulted in rocking about the y axis and it is the highest amplitude flexible response for demonstrating filter performance.
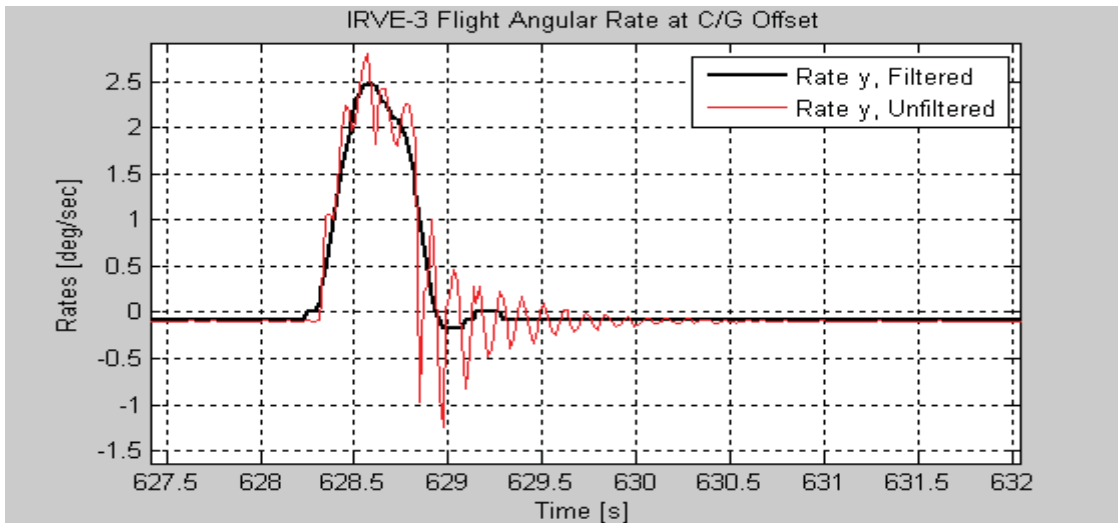

Figure 10: Filtered and raw y axis rate at C/G offset.

In flight, however, the aeroshell came to full inflation pressure quickly, and was at 18psi at T+587 seconds. The observed frequency of the rate oscillations is approximately 9.5 Hz and stable for the full control period suggesting that the preflight predictions and measurements were accurate and that the aeroshell was at full stiffness when the ACS began control.
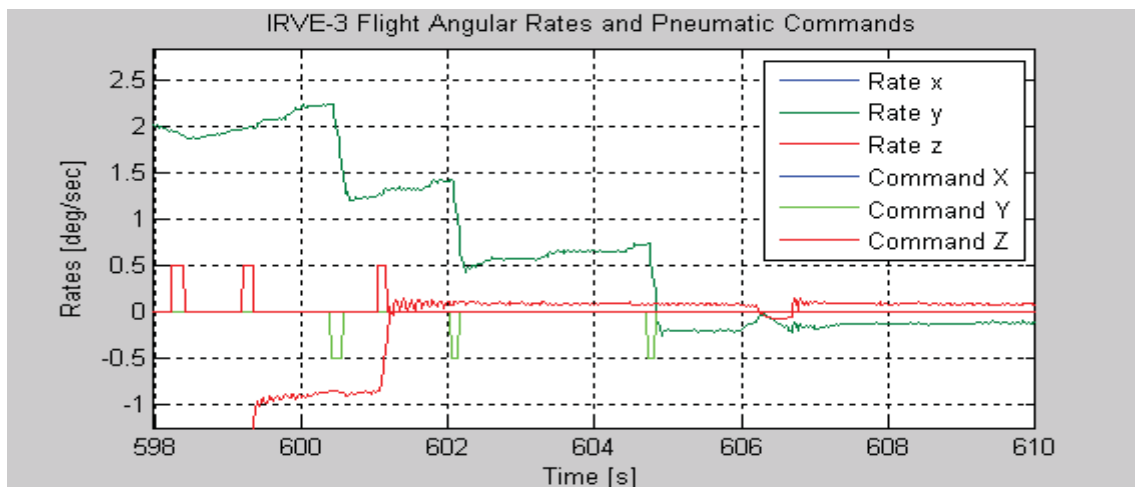

Figure 11: Flexible response, more pronounced in the 0-180 axis, NIACS Z, unfiltered.

10

The alignment was completed and the payload was well stabilized by T + 620 seconds. The ACS control was disabled between 627 and 630 seconds for the offsetting of the payload center of gravity. The payload contained a module that allowed the translation along the NIACS Z axis of the aft end of the payload with respect to the forward end. The two sections translated 1.5 inches with respect to each other. This can be seen at T+628 seconds.
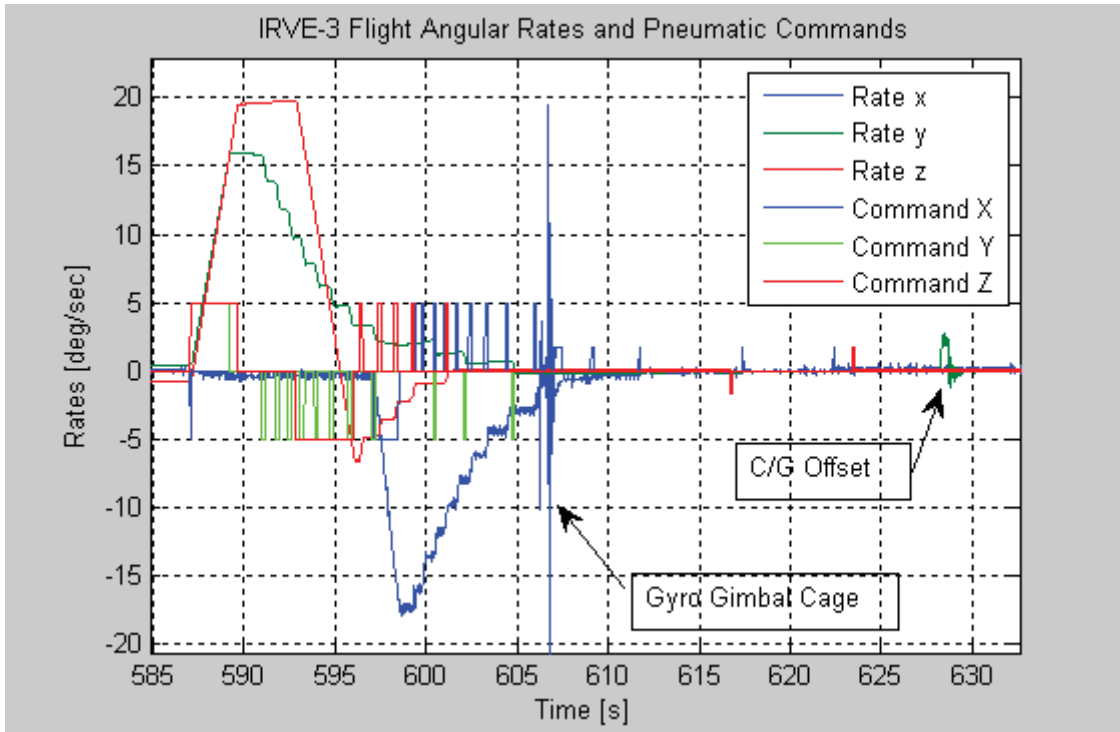

Figure 12: 3 axis rates.

In order to allow 3-axis pointing control on the payload until the beginning of reentry, the ACS switched to altitude based maneuver advancement at T+645 seconds. This was the 2 sigma predicted early time that the payload would cross 88 kilometers on the down leg for a nominal trajectory direction. Due to the as-flown southerly direction of the trajectory and the spherical Earth model used to estimate altitude the system switched properly at an altitude measure of 86.3 kilometers from 3-axis control to roll-only control at T+663 seconds. At this time the payload is traveling at a velocity of 2.7 kilometers per second. This proved to be a very good switching altitude; in Figure 13 the ACS is seen reacting to the building atmospheric disturbance beginning at 660 seconds. Pointing control is disabled just as the disturbance builds. By T+667 seconds, the external disturbance was greater than the control authority of the ACS and any pneumatic activity would have wasted control gas without being able to improve the entry attitude.
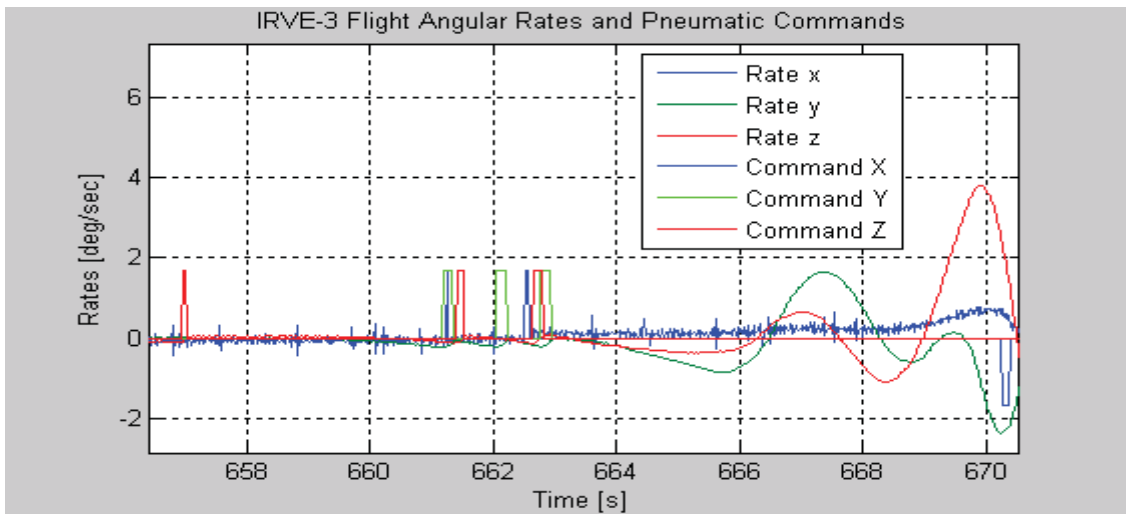
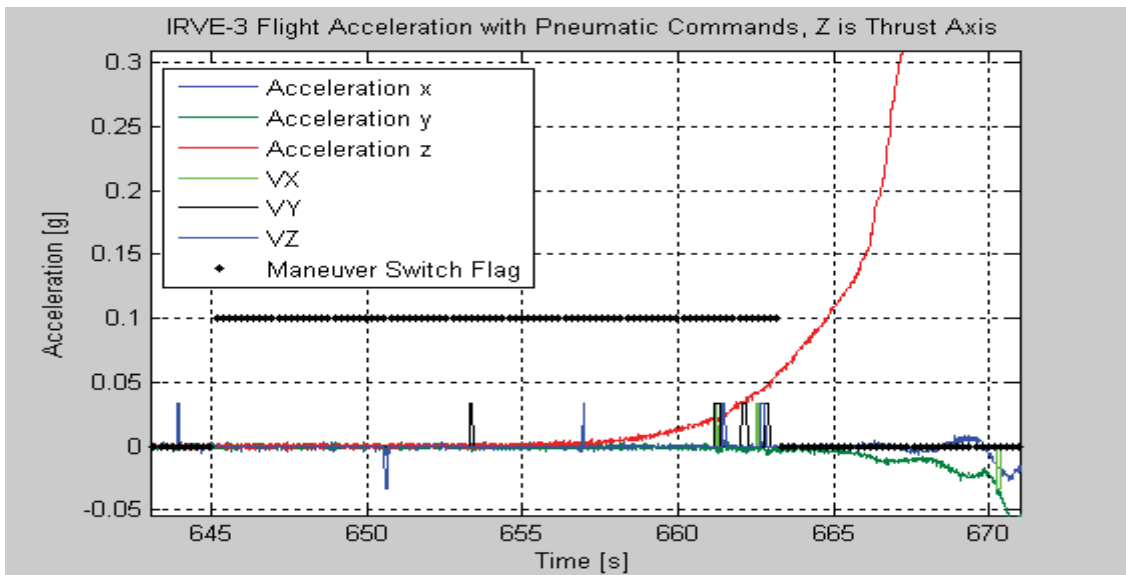**Figure 13: Rates and pneumatics at atmospheric interface.**

Figure 14: Accelerations and target switching flag.
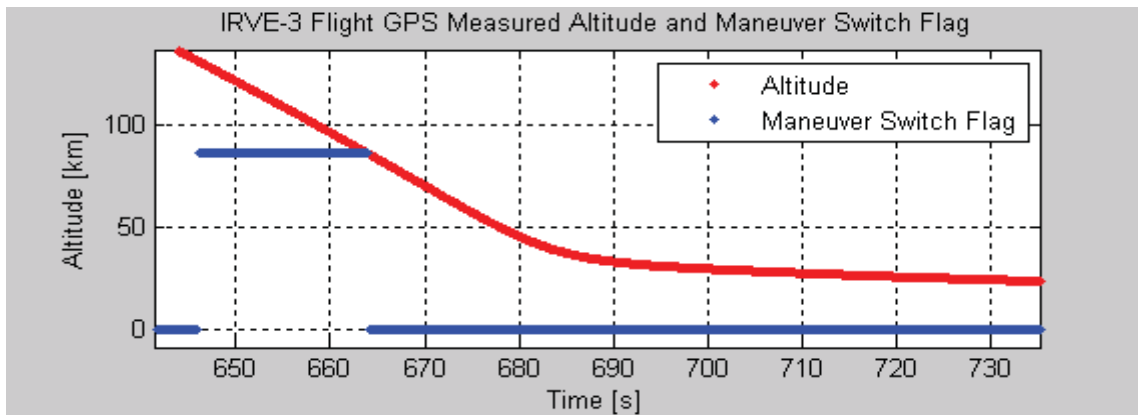

Figure 15: Altitude switch flag, precise altitude reported by GPS 86.24 km.

Entry and Endoatmospheric Control

Reentry began at T+663 seconds as the payload crossed 86.3 kilometers. The control switched to roll-only control to hold the desired roll orientation to within +/- 5 degrees. All available analysis suggested that the ACS had about a 70% chance to hold the roll orientation without being overcome by external disturbances from reentry. The likelihood of experiment success was predicted through Monte Carlo analysis that varied the behavior of the aeroshell during entry. The stiffness and shape of the aeroshell were the strong drivers for successful attitude control. Had the aeroshell deformed asymmetrically, the resultant aerodynamic torques would have exceeded the control authority of the ACS. The aeroshell held shape well and the disturbance was on the mild side of predictions. The maximum roll error during the main experiment was just over 3 degrees; this error is navigated error sensed by the ACS, slightly different from absolute error due to sensor and misalignment errors.
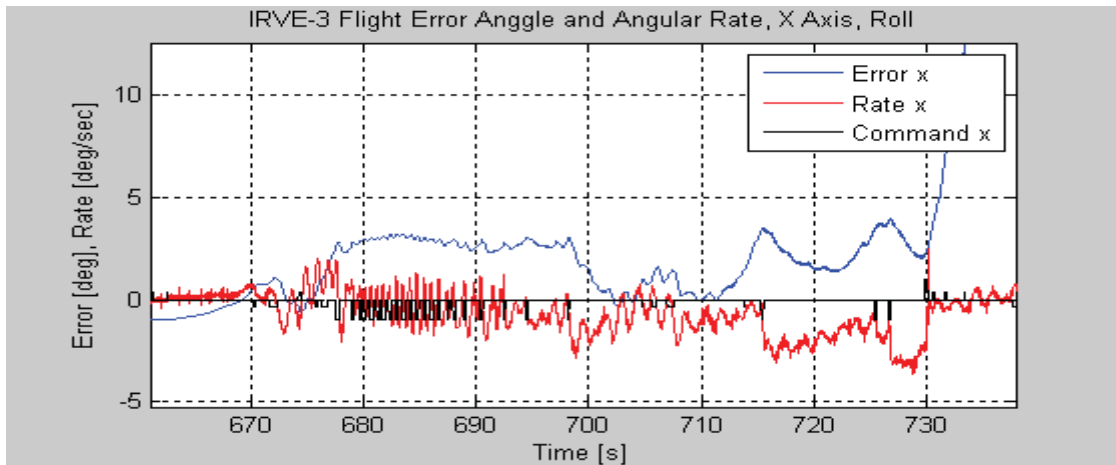

Figure 16: Roll rate and error during entry.

At T+730 seconds, the roll control switched to roll rate damping to prevent a large buildup of roll rate while the C/G offset was actuated 4 more times driving the aft end of the payload back and forth along the 0-180 axis. This was done to observe changes to the angle of attack and the resultant direction of lift due to C/G offset.
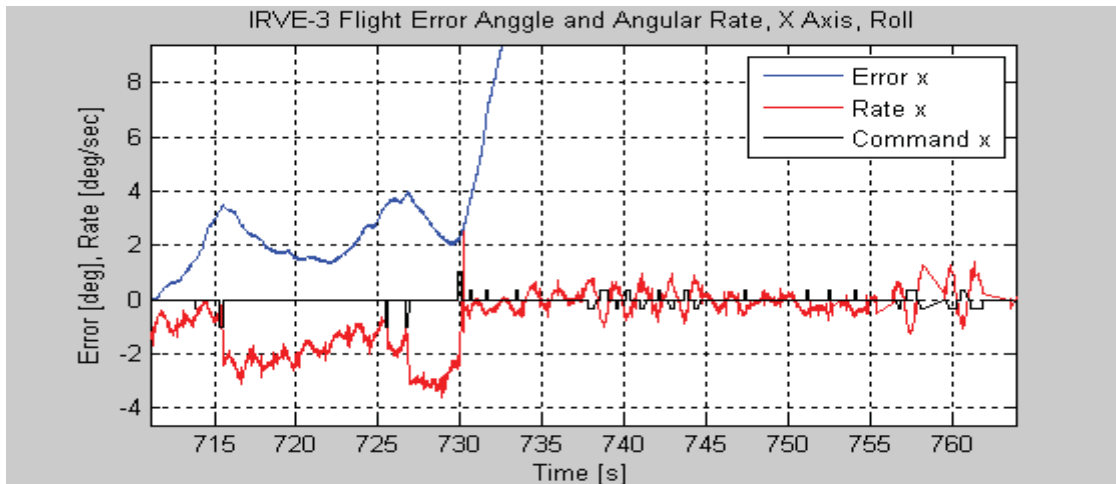

Figure 17: Rate damping for extra credit maneuvers.

Pneumatics

The pneumatics performance was well within preflight expectations. The desired pressures were set preflight and the resulting thrusts and accelerations are compared from the flight data. All flight accelerations are within the expected bounds. The pitch and yaw accelerations are all within 5% of the desired values, and the roll accelerations are all within 10%.
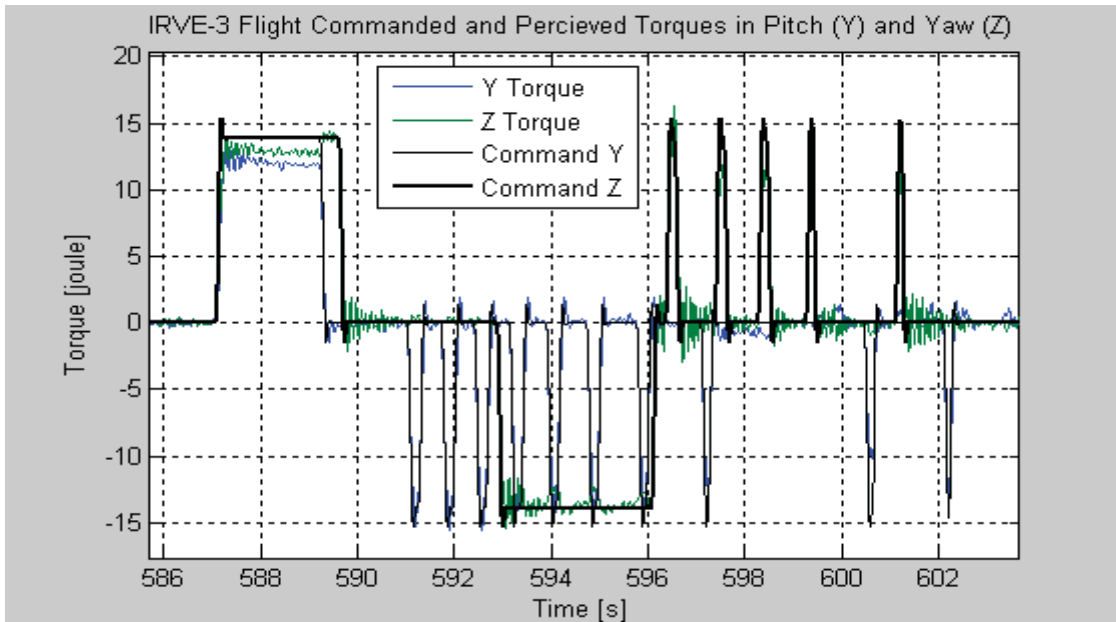

Figure 18: Commanded (black) and measured (color) pitch and yaw torques.

The flexible response of the aeroshell can be seen in the blue and green measured torques. The red measurement is about the NIACS Z axis which is payload 0-180 and the axis of travel of the C/G offset.
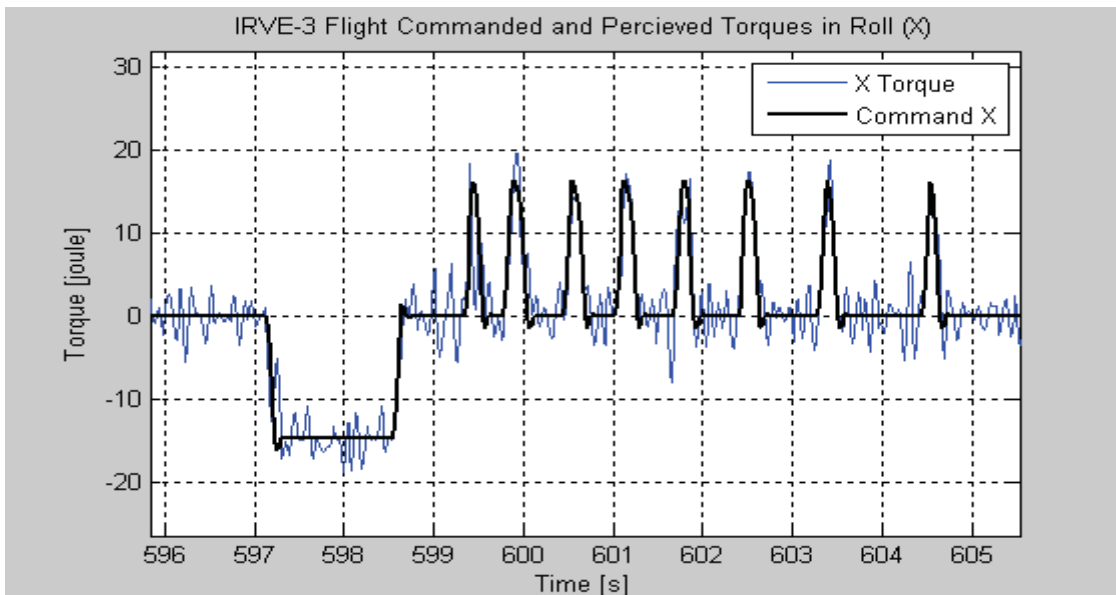

Figure 19: Commanded and measured roll torques

14

The pneumatics delays through the system were measured several times on the air bearing before flight. The pneumatics all demonstrated an on-delay of 20 to 30 milliseconds between command and realization of applied thrust. The pitch and yaw pneumatics circuit demonstrated an off-delay between 20 and 40 milliseconds and the roll demonstrated on off-delay between 60 and 80 milliseconds. The extra roll delay was attributed to the plumbing between the roll valves and nozzles. The technique from which the above plots were taken was used to find the in-flight pneumatics delays. This technique uses the measured payload rates and the pneumatic commands and passes them both through the same filters to allow for a very clean rate measure without adding filtering time delays between the rates and the commands. The results are perceived torques on the payload body which can be compared to the pneumatics commands. This method showed a global delay in both on and off of 40 milliseconds. It is important to note that the pneumatics are commanded at 50 Hz and the data used for this analysis was also reported at 50 Hz so the results have a 20 millisecond uncertainty. The flight will be further compared to the air bearing to better understand whether the current work is underestimating a roll off-delay or the preflight work over estimated that delay.

The onboard gas is depleted as expected well after the extra credit maneuvers, and the system is vented fully through the vent command. After the initial alignment to the velocity vector, the main tank pressure is seen to increase as the gas warms after being cooled during control. The initial increase is typical, however; at the start of atmospheric entry the pressure begins to increase at a faster rate. This is suspected to be due to increasing heat transfer on entry but there are no tank mounted thermistors making it impossible to be certain. It is also expected that this shows an exaggerated temperature rise compared to the actual tank temperature due to the tubing that feeds that transducer being mounted very near the skin so that as the air thickens, the heat transfers quickly from the skin to the tube.
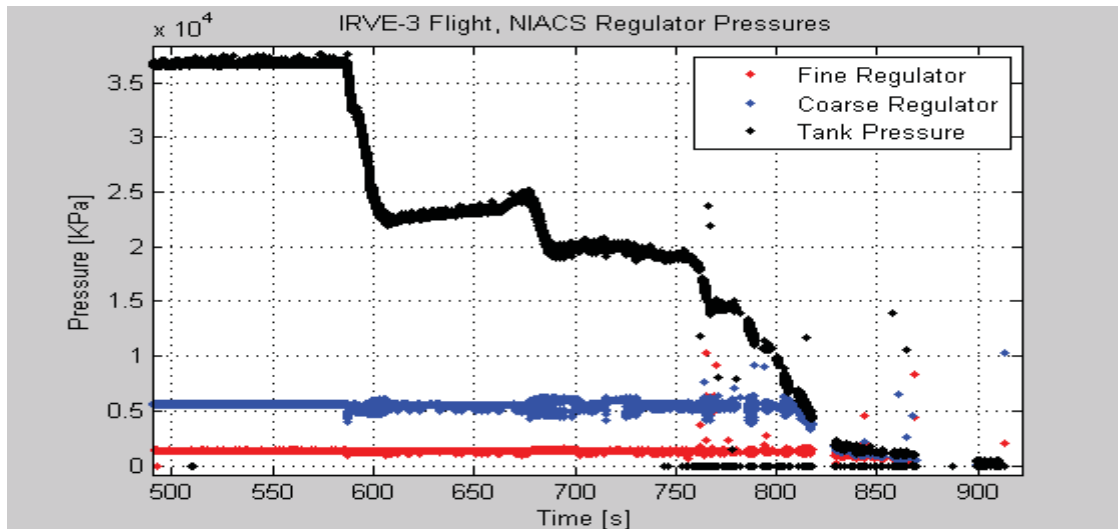

Figure 20: Tank and regulated pressures, full flight.

The impulse used was measured based on valve on-time and corrected for flight measured thrusts. This measure was compared to the simulated gas consumption when flight conditions are fed into the simulation. The comparison is favorable, but the method used to integrate the consumed impulse is calculated in the same manner for each, valve on-time multiplied by thrust, so a favorable comparison is expected. The experiment and extra credit maneuvers were completed with 50% of the available impulse remaining.
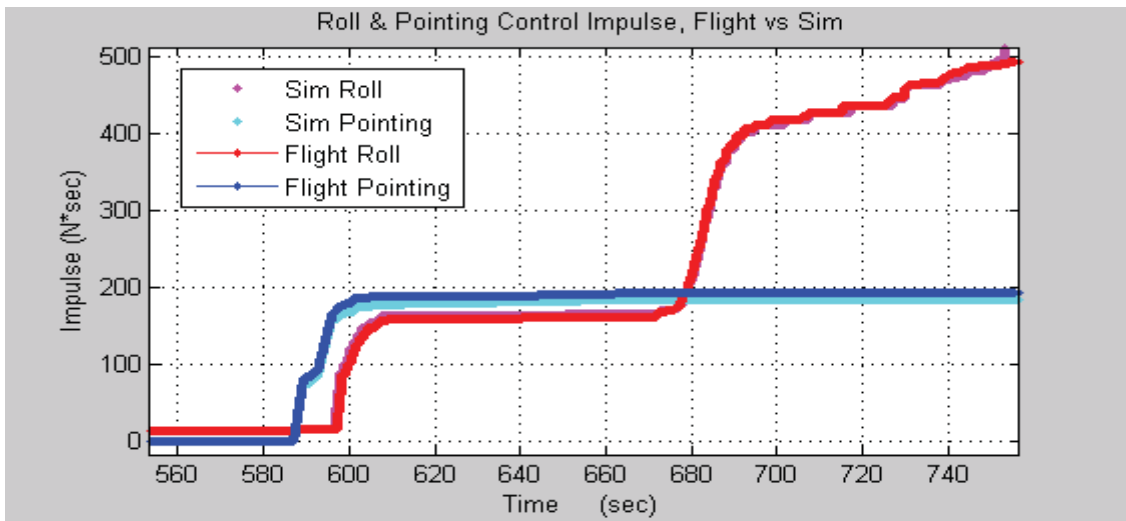
Figure 21: Impulse used

Without a measure of the gas temperature it is impossible to determine the percentage of gas lost during control. If the assumption is made that at T+750 seconds the tank temperature is stable, and the preflight prediction of 1360 N-sec of total impulse is correct, then the impulse used by T+750 seconds is 681 N-sec based only on pressure decrease. The thrust integration across valve on-time method reports a total impulse used at T+750 seconds of 685 N-sec. These numbers are similar and suggest that the current methods used for calculating gas budgets are sound.

COMPARISON TO PREFLIGHT SIMULATION

An initial post flight simulation is presented. Only the initial alignment to the velocity vector is shown for all three axes. The experiment through T+730 seconds is shown for roll. Much work was done preflight to simulate the ACS control using software at Langley Research Center. The simulation comparisons presented here are between the flight results and the NSROC simulation.
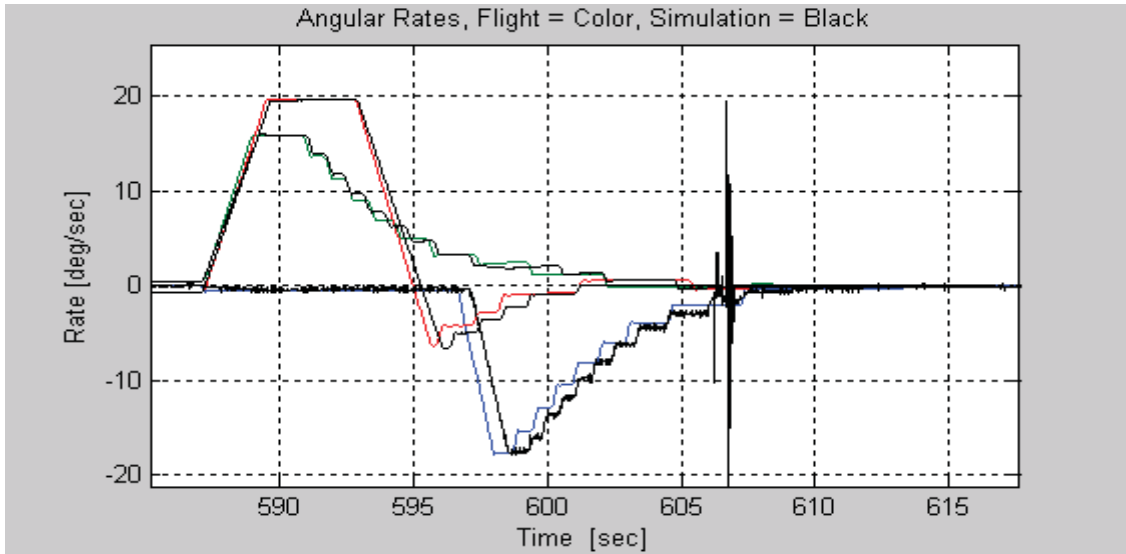

Figure 22: Simulation to flight comparison, rates at initial convergence.
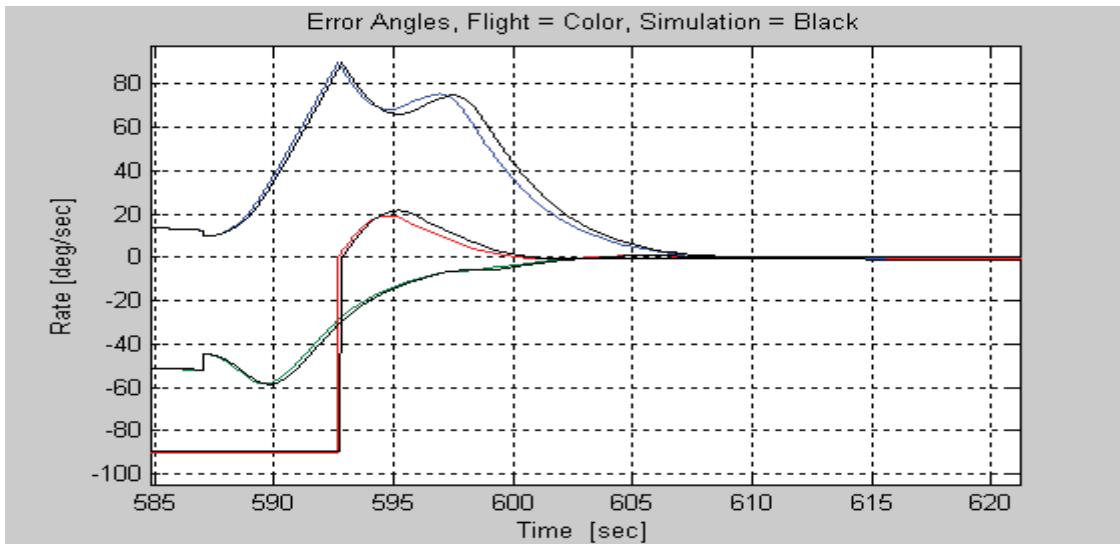
16

Figure 23: Simulation to flight comparison, errors at initial convergence.

The roll performance during entry is compared below. The flight-measured targets are fed into the simulation and the flight measured initial conditions and attitude at T+580 seconds are also programmed into the simulation. The external roll torque on the centerbody is estimated by the reported gyro rate and that torque is also fed into the simulation. The comparison is favorable.
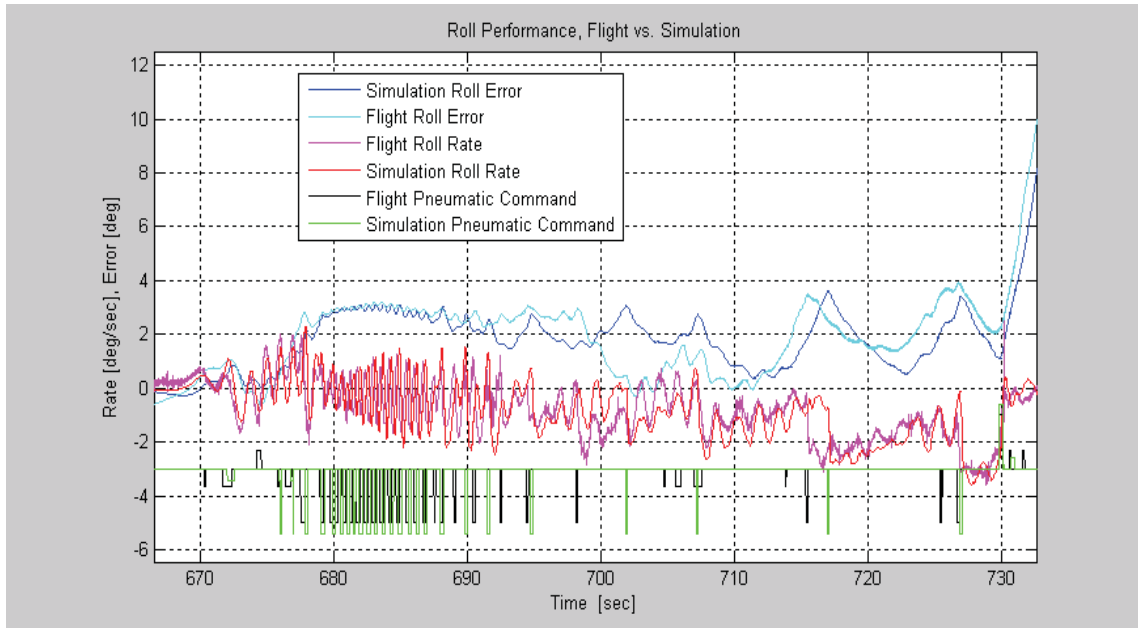

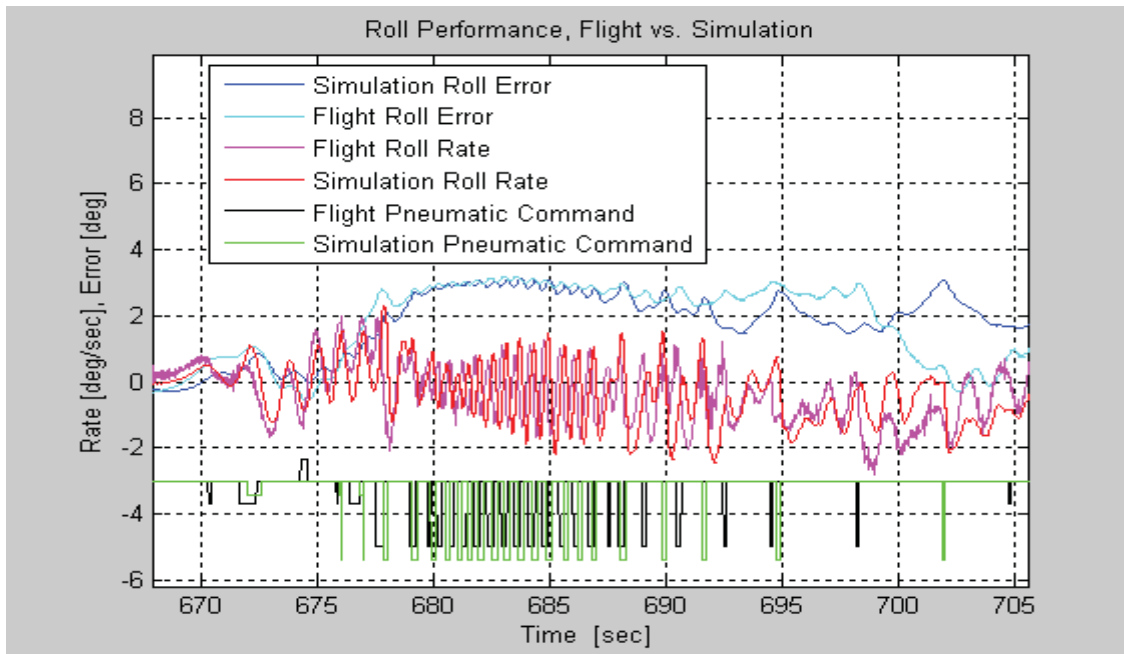**Figure 24: Roll performance during entry.**

Figure 25: Close up of entry sim comparison.

There is a significant amount of continued post flight simulation work to be done. The comparisons shown above are good, but the ability to configure the simulation to read the exact flight environment should allow for a near exact comparison. In addition, the flight effects of plume impingement between the ACS jets and the aeroshell will be examined. To date, no evidence has been seen from the flight data to suggest that there were any negative effects from plume impingement.

CONCLUSION

The successful flight of IRVE-3 demonstrated that HIADs can withstand their intended reentry heating environment, and gathered flight data on the effects of static and dynamic CG offsets on reentry trajectory of such vehicles. This data will be used in future HIAD technology development efforts, including possible demonstration flights where a HIAD either could be maneuvered to a desired landing site using an active CG offset system, or could be used for recovery of a payload from low Earth orbit.

The successful performance of the NIACS during the IRVE-3 mission proved once again the robustness of the design, and also illustrated that the broad capabilities of the system allow it to be used on a wide variety of missions without substantial redesign. It is planned for use on many additional flights in the future.